Conformational Control of Photoinduced Charge Separation within Phenothiazine−Pyrene Dyads

André Stockmann,[†] Jana Kurzawa,[†] Norbert Fritz,[†] Nursel Acar,[†] Siegfried Schneider,*[,†] Jörg Daub,[‡,⊥] Raimund Engl,[‡] and Timothy Clark[§]

Institut für Physikalische und Theoretische Chemie, Friedrich-Alexander-Universität Erlangen-Nürnberg, D-91058 Erlangen, Germany, Institut für Organische Chemie, Universität Regensburg, D-93040 Regensburg, Germany, and Computer-Chemie-Centrum, Friedrich-Alexander-Universität Erlangen-Nürnberg, D-91052 Erlangen, Germany

Received: November 20, 2001; In Final Form: April 5, 2002

Electron donor−acceptor systems, in which phenothiazine is tethered to pyrene by means of a phenyl bridge, exhibit a dual emission in moderately and very polar solvents. Employing steady-state and time-resolved fluorescence spectroscopy, we were able to provide evidence that the "blue" and "red" emission bands originate from different conformers. The ground-state geometry of the majority species is identical to that found in the crystalline state (the quasi-equatorial conformer). This conformation executes a fast electron-transfer process accompanied by significant structural relaxation. Consequently, its fluorescence exhibits a large solvatochromic shift typical for charge-transfer states. The photophysical properties of the minority species (the quasi-axial conformer) vary significantly with the substitution pattern of the bridging phenyl ring. In part, this difference is related to the orientational factor, κ, governing the rate of energy transfer between the pyrene and phenothiazine moieties. In the para-substituted derivative, fluorescence emission from both the excited phenylpyrene and the phenylphenothiazine subsystem can be observed. In the meta-substituted derivative, fluorescence originates mainly from the primarily absorbing phenylpyrene subsystem. In nonpolar solvent (cyclohexane), the nature of the fluorescing state differs for the para- and meta-substituted compounds. Whereas in the former, the fluorescence originates from the locally excited phenothiazine, it is governed by emission from a structurally modified CT state in the latter derivative. Semiempirical (AM1/CI) molecular orbital calculations with a continuum solvent treatment have been used to investigate the different states involved and provide explanations for the observed results. The calculations reveal the existence of an intermediately populated CT state in which the negative charge is partly localized in the bridge as well as in the pyrene acceptor.

1. Introduction

In the last 10 years, numerous investigations aimed at a better understanding of (photoinduced) intramolecular electron transfer[1−15] and especially at the correlation between the rate of this process, k_{et}, and the overall geometry of the donor−bridge−acceptor (D−B−A) system have been reported. However, the spatial arrangement of donor and acceptor was only uniquely fixed in the electronic ground state and also conserved in the electronically excited states, from which electron-transfer started, in a very few cases.[16,17] Nevertheless, many attempts have been made to explain variations in the rate of electron transfer, k_{et}, e.g. upon variations of the donor−acceptor distance assuming a specific conformation of the bridge. More recently, it has become clear that conformational parameters such as rotation around a single or double bond or folding of a semiflexible bridging element like a piperidyl ring, which alter both distance and relative orientation of donor and acceptor, can be decisive factors for the photophysical properties of charge-transfer states.[18,19] Because of the difference in Gibbs energy required for charge separation and recombination in different conformers, the two processes can occur with greatly different rates.[20] They are, in addition, sensitively dependent on solvent polarity, whenever the distance for charge separation varies significantly between different conformers. An interesting structural element, which can lead to pronounced conformational heterogeneity in the electronic ground state, is a nitrogen heterocycle, for which the substituent (bridging element) can adopt a quasi-axial or quasi-equatorial position.[21] Moreover, it has been proposed that the hybridization of the nitrogen will change upon electronic excitation. In the case of complete electron withdrawal (oxidation) the nitrogen can even adopt a planar geometry (sp^2 hybridization).[22]

In the electronic ground state, the stereochemistry of, e.g., N-substituted phenothiazines is by no means clear. Obviously, it can change with the nature and size of the substituent, thus leading to a majority species (the thermodynamically most stable) and one or more minority conformers. A priori, it is difficult to predict how different the photophysical and photochemical properties of the various conformers are. This implies that minor changes in the structure of the substituent can induce a shift from one majority conformer to another. Consequently, any attempt to explain results on the basis of only one selected conformation is likely to fail.

* Corresponding author. E-mail: schneider@chemie.uni-erlangen.de.
[†] Institut für Physikalische und Theoretische Chemie, Friedrich-Alexander-Universität Erlangen-Nürnberg.
[‡] Universität Regensburg.
[§] Computer-Chemie-Centrum, Friedrich-Alexander-Universität Erlangen-Nürnberg. E-mail: clark@chemie.uni-erlangen.de.
[⊥] E-mail: joerg.daub@chemie.uni-regensburg.de.

10.1021/jp0142987 CCC: $22.00
Published on Web 08/07/2002

SCHEME 1: Chemical Structures of Compounds Investigated and Abbreviations Used

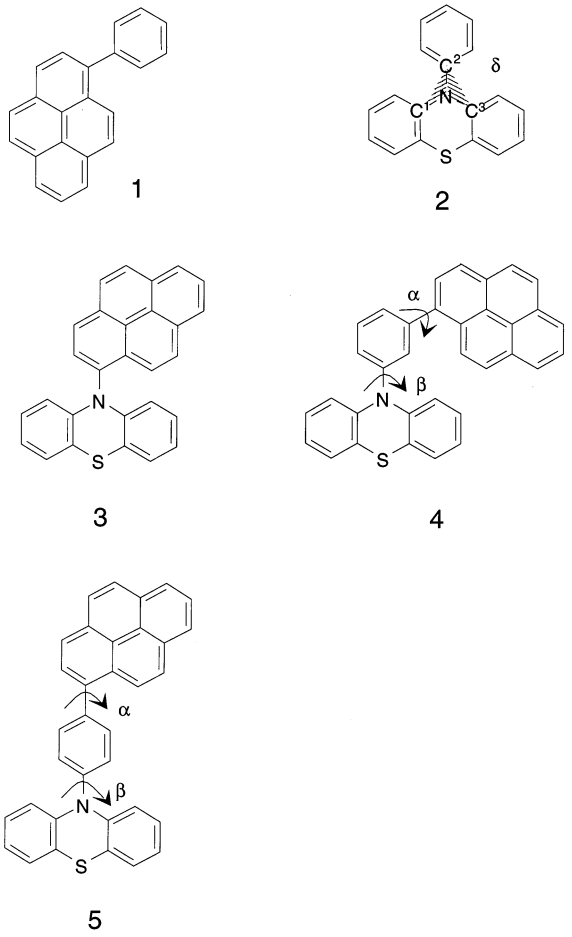

In two previous publications, we reported the results of transient absorption[17] and Raman experiments[23] performed with D−B−A systems comprising phenothiazine as donor, pyrene as acceptor, and a phenyl ring as bridging element (see Scheme 1; to avoid confusion, the abbreviations used are the same as in the preceding publications). The results of both types of experiments provided evidence that photoinduced electron transfer occurs with rate constants on the order of $k_{et} \approx 10^{11}$ s^{-1}. The magnitude of the rate implies that fluorescence from locally excited (LE) states, which are precursors of the charge-transfer (CT) states generated, should be heavily quenched. Nevertheless, one observes a fairly strong fluorescence in the spectral region, in which fluorescence originating from the LE states is expected. We therefore hypothesized that the compounds investigated exist in solution in two forms: (i) as a majority species, whose conformation is the same as that found in crystalline material by X-ray analysis and which is also predicted by quantum chemical model calculations as the minimum energy conformation, and (ii) as a minority species, which represents a local energy minimum in quantum chemical calculations. The latter conformer has been suggested to be responsible for the appearance of "blue" fluorescence in (moderately) polar solvents next to the polarity-dependent "red" CT fluorescence.

In this contribution, we present the results of steady-state and time- and wavelength-resolved fluorescence measurements and discuss the influence of the bridging pattern on the photophysical and photochemical properties of phenothiazine−pyrene dyads by comparison with the results of quantum chemical model calculations.

2. Materials and Methods

2.1. Materials. The synthesis of the compounds has been described in detail elsewhere.[17,24] The usual analytical techniques were employed to test the purity of the samples. No indication for the presence of impurities or unreacted starting materials could be found. All solvents were spectroscopic grade and used as supplied (Aldrich). Sample solutions (concentration of solutes was $\leq 5 \times 10^{-5}$ M to avoid excimer formation) were freed from oxygen by bubbling through with argon for about 20 min prior to fluorescence measurements at $T = 298$ K.

2.2. Experimental Methods. UV/vis absorption spectra were recorded on a Perkin-Elmer Lambda 2 spectrometer, steady-state emission spectra at ambient temperature on a Perkin-Elmer LS 50B. The recorded emission spectra were corrected for the spectral sensitivity of the detection channels. The latter was determined by comparison with the known emission characteristics of a 1000-W tungsten lamp (EG & G, model 590-20). The actual values of the excitation or detection wavelengths are given in the legends to the figures.

The time- and wavelength-resolved fluorescence experiments employed a setup developed originally by EuroPhoton[25] (Berlin, Germany). We later modified it to suit our specific needs better.[26] The system relied on the well-known technique of time-correlated single photon counting. By replacing the conventional multichannel plate (MCP) photomultiplier with one containing a so-called delay-line anode (model EMI-132 N300, ELDY, Petersburg, Russia), one can deduce information about not only the arrival time of the fluorescence photon but also its wavelength.[25] In combination with a two-dimensional multichannel analyzer, one obtains as raw data the intensity distribution $I_F(\lambda,t)$. The wavelength increment per channel is 1.5 nm for the spectrograph employed (Oriel, model MS125); the time increment is either approximately 12 or 48 ps, depending on the setting of the time-to-amplitude converter (TAC). To reduce the amount of data, and to facilitate the curve-fitting procedure, the content of 20 neighboring channels was usually binned to produce about 10−15 decay curves $I_F(\lambda_j,t)$ for each spectral segment $\lambda_j \pm \Delta\lambda_j$ covered by a specific wavelength setting of the spectrograph. Single-curve and multicurve fitting was performed in the usual manner employing least-squares fitting techniques based on the Marquardt and Simplex algorithms.[27] The recorded fluorescence intensity distribution $I_F(\lambda_j,t)$ represents the convolution of the excitation profile $E(t)$ with the fluorescence decay law $R(\lambda_j,t)$:

$$I_F(\lambda_j,t) = E(t - t_0) \otimes R(\lambda_j,t)$$

where t_0 represents a possible shift of time zero when scattering solution and sample are exchanged. In the assumed multiexponential decay law

$$R(\lambda_j,t) = \sum A_i(\lambda_j) \exp(-t/\tau_i)$$

$A_i(\lambda_j)$ represents the amplitude of the ith lifetime component for detection wavelength λ_j.

For excitation at $\lambda_{ex} = 277$ nm, the frequency-tripled output of a home-built Titan:sapphire laser[28] with cavity-dumper pumped by a Millennia (Spectra Physics) CW Nd:YAG laser was used ($t_p \approx 100$ fs, repetition rate 800 kHz). Standard NIM electronic components were used in the detection circuit. The system response function measured via scattering of the laser pulse is determined by that of the MCP photomultiplier and showed about 50 ps full-width at half-maximum. Generally, 10^7 fluorescence events were monitored per measurement. (More

experimental details can be found in the PhD thesis of A. Stockmann.[27])

To speed up the global fit procedure, a new algorithm was developed in which single-curve fits and multicurve fits are performed alternately. After an initial multicurve fit to obtain good starting values for the global parameters (lifetimes τ_i and shift t_0), all fits of the individual decay curves $I_F(\lambda_j,t)$ were optimized with respect to the remaining parameters not considered as global parameters (e.g., amplitudes $A_i(\lambda_j)$). The total χ^2 is calculated as sum of the ${\chi_j}^2$ of the individual curve fits and used as a criterion for the modification of the global parameters in the following multicurve fit procedure. With the new set of global parameters (lifetimes), all decay curves are fitted again individually yielding a new set of ${\chi_i}^2$ values and concomitantly the total χ^2 of the next iteration step. It proved advantageous to perform the multicurve fits with the Simplex algorithm, and the single-curve fits by means of the Marquardt algorithm with an additional Simplex optimization.[29]

2.3. Quantum Chemical Model Calculations. Calculations were performed by using the program package VAMP 8.0.[30] Molecular properties in the electronic ground state were computed by using the restricted Hartree−Fock formalism with the AM1 Hamiltonian.[31] Excited-state calculations used a singles plus pair doubles (PECI)[32] configuration interaction (CI) expansion with an active window of the four highest occupied and the four lowest unoccupied molecular orbitals. Test calculations with both full CI using the same active orbital window and with a singles-only CI with up to 24 active orbitals suggested that this level of theory is adequate for the problem. Excited-state geometries were optimized in vacuo by using analytical CI gradients.[33] In some cases, the charge-transfer states were separated energetically from local excitations by applying a homogeneous electrostatic field during the early stages of the geometry optimizations in order to avoid state crossings during the optimization. Final optimizations were performed without external fields. Solvent effects were simulated in single-point calculations on the gas-phase optimized geometries by using our polarized continuum solvation model[34,35] with natural atomic orbital−point charge (NAO−PC) electrostatics[36] but without the dispersion contribution reported originally.[34] The self-consistent reaction field calculations used solvent-excluded surfaces[37] with atomic radii equal to 120% of those given by Bondi.[38]

3. Results and Discussion

3.1. Steady-State UV/Vis Absorption and Emission Spectra. Introduction of the phenyl substituent causes the pronounced vibronic structure seen in the UV/vis absorption spectra of pyrene to disappear, Figure 1a. The long-wavelength slope of the $S_0 \rightarrow S_2$ absorption band of phenylpyrene is bathochromically shifted by about 15 nm, thereby reducing the difference to the still very weak $S_0 \rightarrow S_1$ absorption band around 375 nm. In the case of phenothiazine, phenyl substitution also causes a bathochromic shift of about 15 nm of the $S_0 \rightarrow S_1$ absorption band and reduces the corresponding ϵ_{max} by a factor of nearly 2. This implies that above 275 nm the absorption of phenylpyrene exceeds that of phenylphenothiazine by far, except in a small wavelength range around 295 nm. The fluorescence spectrum of phenylpyrene exhibits an approximate mirror image to the strong absorption band, showing maxima at about 380 and 395 nm. The fluorescence spectrum of phenylphenothiazine exhibits a very large Stokes shift of about 125 nm, the emission maximum being found around 450 nm in CH_2Cl_2. This unusually large Stokes shift is indicative of large structural changes occurring during the excited-state lifetime.

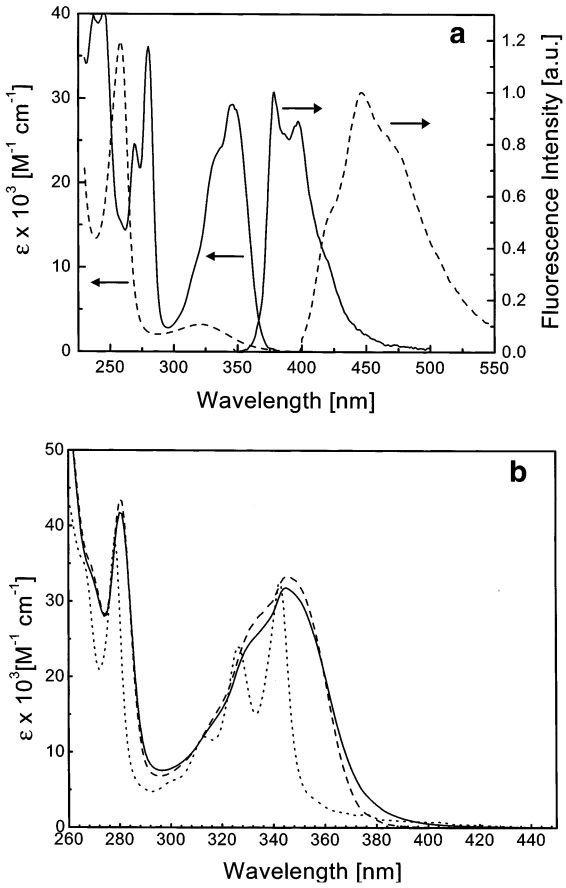

Figure 1. (a) UV/vis absorption and emission spectra of phenylpyrene, **1** (λ_{ex} = 340 nm) (−), and phenylphenothiazine, **2** (λ_{ex} = 300 nm) (- - -), in CH_2Cl_2. (b) UV/vis absorption spectra of investigated compounds in CH_2Cl_2: **3** (· · ·), **4** (- - -,) and **5** (−).

Since the UV/vis absorption spectra of the D−B−A systems were found to be fairly independent of solvent polarity, we restrict our discussion to the spectra recorded in CH_2Cl_2, Figure 1b. The absorption spectrum of the directly linked system **3** exhibits a pronounced vibrational structure like the parent pyrene. This observation provides evidence that the π-electronic systems of pyrene and phenothiazine are essentially orthogonal to each other. In the phenyl-bridged systems **4** and **5**, the vibrational structure has essentially disappeared. The spectra resemble that of phenyl-substituted pyrene (Figure 1a). Based on the X-ray structures of **4** and **5**, and the results of MO calculations, the lack of vibrational structure is explained by π-conjugation made possible by a torsional angle of the phenyl−pyrene bond of only about 60°. Noteworthy is the long tail of the red absorption band extending beyond 400 nm. It could be due to an increase of the extinction coefficient of the $S_0 \rightarrow S_1$ absorption of pyrene as a result of the symmetry reduction caused by the substituent. This explanation is, however, unlikely, since the effect should also show up in phenylpyrene. Alternatively, a weak transition from the ground state to a charge-transfer state can be considered.

Both **4** and **5** exhibit a dual emission in moderately and very polar solvents, Figure 2. In contrast to other examples, in which strongly quenched emission from the locally excited precursor state and solvent-polarity-dependent long-wavelength emission from the charge-separated state are observed, the blue emission found in the most polar solvent (acetonitrile) appears relatively more intense than that in the less polar solvent CH_2Cl_2. Also surprising at first glance is that in the meta-substituted compound **4**, the fluorescence maximum observed in cyclohexane lies at

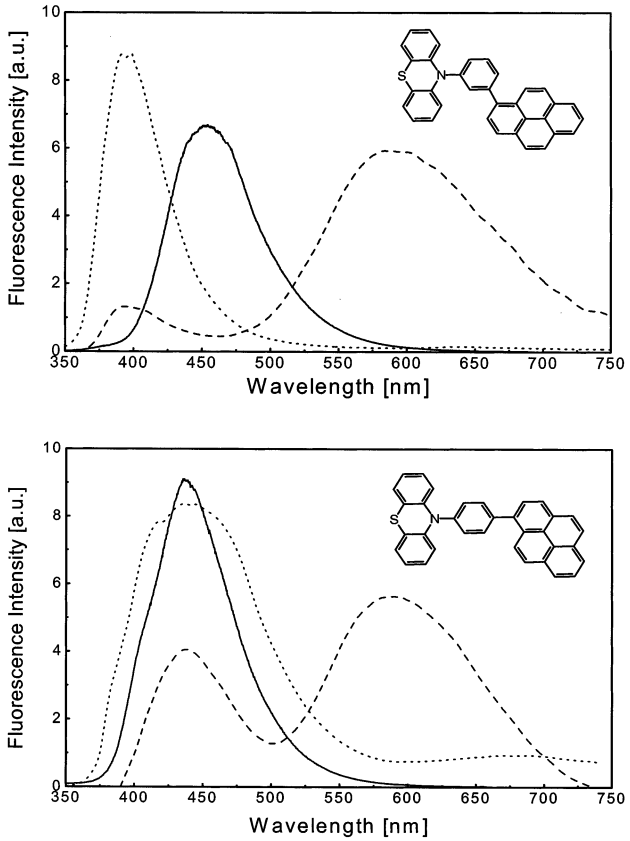

Figure 2. Steady-state fluorescence spectra of (top) **4** and (bottom) **5** in different solvents: cyclohexane (—), CH_2Cl_2 (- - -), and acetonitrile (. . .). Excitation wavelength $\lambda_{ex} = 300$ nm.

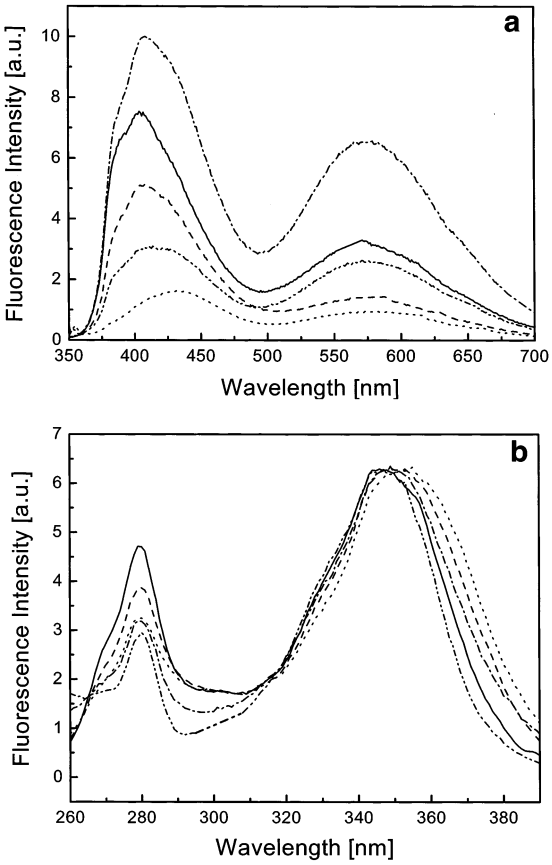

Figure 3. (a) Dependence of the steady-state fluorescence spectra of compound **5** in CH_2Cl_2 on excitation wavelength. $\lambda_{ex} = 280$ nm (—), 287 nm (- - -), 300 nm (• • •), 320 nm (- • • -), and 345 nm (- • -). (b) Fluorescence excitation spectra recorded for **5** in CH_2Cl_2 for various observation wavelengths: $\lambda_{obs} = 400$ nm (—), 425 nm (- - -), 450 nm (• • •), 500 nm (- • -), and 600 nm (- • • -). For easier comparison, the spectra are normalized at the red maximum.

longer wavelength than that of the blue emission in acetronitrile. The para-substituted derivative **5** shows the emission maxima in both solvents at about the same wavelength. Noteworthy is, however, the much larger width of the blue band in acetonitrile (ACN).

The ratio of the intensities of the blue and red emission bands varies not only with solvent polarity but also with excitation wavelength, as demonstrated for the para-derivative **5** in Figure 3a. It is immediately obvious that the blue emission is relatively weaker for $\lambda_{ex} = 345$ or 320 nm, where absorption is dominated by that of pyrene. Excitation around the valley at about 297 nm produces relatively more intense blue fluorescence. Furthermore, the spectral distribution of the blue emission varies somewhat with excitation wavelength. Excitation in the long wavelength tail ($\lambda_{ex} = 392$ nm) yields a dominant blue fluorescence, with a phenothiazine-like emission ($\lambda_{max} = 445$ nm).

An excitation-wavelength-dependent emission spectrum is generally taken as evidence for a heterogeneous sample with more than one absorbing and emitting species. In our case, the emission spectra of the (two) species cannot overlap much because the spectral distribution within the red and blue bands hardly changes with excitation wavelength. A possible explanation could therefore be that one of the absorbing species emits predominantly from the locally excited state(s), whereas the other undergoes rapid electron transfer and emits preferentially from the CT state generated. The rate of formation of the CT state in **4** and **5** was determined to be on the order of 10^{11} s^{-1}.[17,23] By comparison with the fluorescence lifetime of phenylphenothiazine ($\tau_F \sim 3$ ns), the fluorescence yield of the LE state of the phenothiazine moiety should be lowered by at least a factor of 100 because of the electron transfer. For the phenylpyrene moiety ($\tau_F \sim 105$ ns), this reduction should be even larger, more than 1000-fold. This implies that LE-type emission from the species that undergoes fast electron transfer should be detectable neither in the steady state nor in the time-resolved measurements.

The hypothesis of different absorbers can be checked readily by recording fluorescence excitation spectra with observation wavelengths in the blue and red fluorescence bands, respectively (Figure 3b). The similarity in the overall appearance of the excitation spectra is in accordance with the assumption that the two absorbing species are different conformers of the same molecular species, which exhibit only slightly different absorption characteristics. A closer look reveals, however, that the onset of the excitation spectrum of **5** is found at the shortest wavelength, if the fluorescence is monitored in the red emission band (550−650 nm). In this case the location of the first maximum in the excitation spectra matches that of the first maximum in the UV/vis absorption spectrum very well. We consider this as evidence that the species that produces the CT fluorescence governs the characteristics of the absorption spectrum and is therefore the dominant (majority) species. If the detection wavelength is chosen below 550 nm, the first maximum in the excitation spectra (and concomitantly the apparent onset) shifts toward longer wavelength. The red-most maximum ($\lambda \approx 352$ nm) is found if the fluorescence is monitored at the maximum of the blue band, i.e., around 450 nm. This implies excitation and emission of the phenylphenothiazine moiety. If the detection wavelength is shifted further

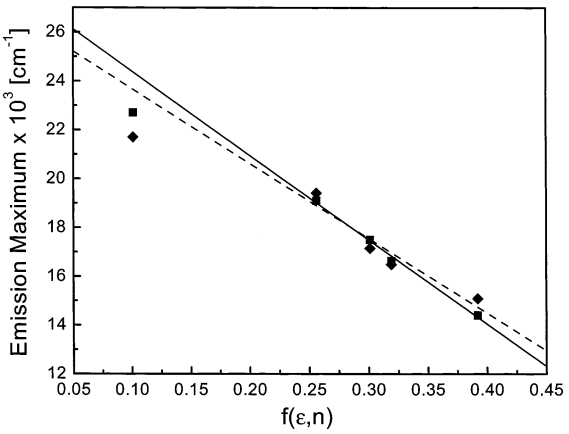

Figure 4. Lippert−Mataga plot of the CT fluorescence emission maxima of **4** (♦, - - -) and **5** (■, —) in different solvents (cyclohexane, diethyl ether, Me-THF, CH_2Cl_2, and acetonitrile). ($f = (\epsilon - 1)/(2\epsilon + 1) - 0.5(n^2 - 1)/2n^2 - 1$). The data points collected for nonpolar solvents are omitted in the linear fit for reasons discussed in the text.

to the blue ($\lambda_{det} < 450$ nm), then the maximum in the excitation spectra is also blue-shifted and the relative intensity of the second band around 280 nm is increased. This is in accordance with the fact that the phenylpyrene moiety fluoresces around 400 nm and exhibits a very intense absorption band around 280 nm. This finding also implies that energy transfer from phenylpyrene to phenothiazine is not 100% efficient in the minority conformation.

From the Lippert−Mataga plot (Figure 4), the red emission can be identified as CT fluorescence by the strong solvent polarity-dependence of its maximum. If changes in polarizability are neglected, the shift of the fluorescence maximum in a solvent with permittivity ϵ and refractive index n can be written as[39]

$$\Delta\tilde{\nu}_F = \frac{1}{4\pi\epsilon_0 hc}\frac{2}{a^3}(\vec{\mu}_E - \vec{\mu}_G)\,\vec{\mu}_E\, f(\epsilon,n)$$

where a represents the radius of the solvent cavity, $\vec{\mu}_G$ and $\vec{\mu}_E$ the dipole moments in the ground and excited electronic states, respectively, and $f(\epsilon,n)$ the solvent polarity parameter:

$$f(\epsilon,n) = \frac{\epsilon - 1}{2\epsilon + 1} - \frac{1}{2}\frac{n^2 - 1}{2n^2 + 1}$$

If only the data points obtained in moderately and very polar solvents are used, then the slope obtained in the Lippert−Mataga plot (Figure 4) for the meta-substituted derivative **4** is smaller than that for **5**, thus indicating (under the assumption of equal cavity radii) a smaller dipole moment in the CT state. This means, in the simplest model, a smaller distance across which electron transfer occurs in **4** versus **5**. By assuming a sphere with a volume equivalent to that of an elliptical cavity matching the molecular dimensions with half axes of 670 and 440 pm for **4** and 900 and 385 pm for **5**, one can derive an estimate for the change in dipole moment between ground and emitting CT state of 25.9 D for **4** and 38.8 D for **5** (for the sake of simplicity, μ_G was chosen as zero). These values are much lower than the ones (Table 1) estimated by adopting the X-ray structure and the assumption of a complete electron transfer between phenothiazine and pyrene.[17] This discrepancy indicates that the net charges are largely delocalized and/or electron transfer occurs across a shorter distance. Because the distance between donor and acceptor, R_{DA}, or the dipole moment of the CT state, enters into the estimate of the change of the Gibbs function, ΔG_{et}, the values given in Table 1 might be somewhat too small.

TABLE 1: Characteristic Parameters of the Compounds Investigated

compd	E_{00},[a] eV	PDF,[b] eV	ΔG_{et},[c] eV, CH	ΔG_{et},[c] eV, CH_2Cl_2	ΔG_{et},[c] eV, ACN	R_{DA},[d] Å	μ_{est},[e] D	[μ^2/a^3],[f] cm^{-1}
4	3.38	0.59	0.12	0.87	1.0	7.85	38	47 500
5	3.38	0.59	0.06	0.85	1.0	8.49	41	71 640

[a] E_{oo} refers to that of phenothiazine. [b] PDF $= e(E_{ox}(D) - E_{red}(A)) - E_{oo}$ measured in polar solvent. [c] Estimate according to Rehm−Weller equation. [d] R_{DA} represents distance between nitrogen of phenothiazine and the center of pyrene in the quasi-equatorial conformer. [e] $\mu_{est} = eR_{DA}$. [f] Derived from Lippert−Mataga plot (Figure 4) by using data points for $f > 0.2$ only.

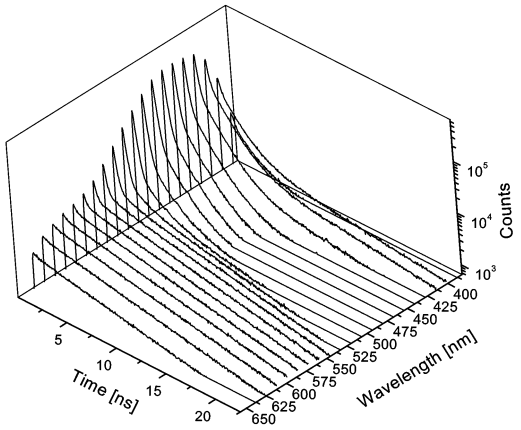

Figure 5. Time- and wavelength-resolved fluorescence decays $I_F(\lambda_j, t)$ recorded for derivative **5** in CH_2Cl_2, $\lambda_{ex} = 300$ nm.

Furthermore, it is noticeable that the emission maxima found in nonpolar solvents (e.g., cyclohexane) do not match the regression line calculated from the data in more polar solvents. This raises some doubt as to whether the emission observed in nonpolar solvents actually originates from a CT state or rather from the LE state(s). Alternatively, it could indicate that the CT state exhibits a different geometry in nonpolar solvents due to large amplitude motions (harpooning effect). In donor−acceptor systems with a nonrigid bridge, this is a well-known phenomenon.[18,19]

3.2. Time- and Wavelength-Resolved Fluorescence Spectroscopy. The time- and wavelength-resolved fluorescence decays shown for derivative **5** as one example in Figure 5 provide immediate evidence that the blue and red emission bands appear immediately after excitation without any measurable delay. For the red emission, this finding is in accordance with the results of the pump−probe experiments, which yielded electron-transfer rates on the order of $k_{et} \approx 10^{11}$ s^{-1}. It is also in agreement with the conclusions drawn from the steady-state fluorescence measurements, namely, that the blue emission does not originate from the precursor state of the red fluorescing CT state.

The analysis of the temporal fluorescence profiles recorded in the farthest red spectral range showed that the CT fluorescence decays monoexponentially with decay times varying between 1 and 11 ns (Table 2). In the spectral range of the blue emission, a proper fit of the fluorescence time profiles needed up to three exponentials. If the spectrally corrected steady-state emission spectra recorded for the same excitation wavelength are used in addition, one can construct the decay associated spectra (DAS) according to

$$\mathrm{DAS}(\lambda_j,\tau_i) = \frac{A_i(\lambda_j)\tau_i}{\sum A_i(\lambda_j)\tau_i} F(\lambda_j)$$

TABLE 2: Photophysical Parameters Determined for the Compounds Investigated from Time- and Wavelength-Resolved Fluorescence Measurements[a]

solvent	property	**1**	**2**	**4**	**5**
cyclohexane	τ_1, ns	124	3.06	8.2	2.8
	λ_{em}, nm		439	450	440
	τ_2, ns			39	0.3
	λ_{em}, nm				425
CH_2Cl_2	τ(CT), ns			11	11
	τ_1(LE), ns	105	3.06	29	21
	λ_{em}, nm	385, 400	450	400	400
	τ_2, ns				1.6
	λ_{em}, nm				412
	τ_3, ns				0.2
	λ_{em}, nm				460
acetonitrile	τ(CT), ns			2.2	1.0
	τ_1(LE), ns	65	2.65	48	30
	λ_{em}, nm		443	400	400
	τ_2, ns			7.3	2.0
	λ_{em}, nm			410	428
	τ_3, ns			1.0	0.07
	λ_{em}, nm			410	470

[a] $\lambda_{ex} = 277$ nm. For compounds **4** and **5**, λ_{em} refers to the maximum in the decay associated spectra of the corresponding lifetime component.

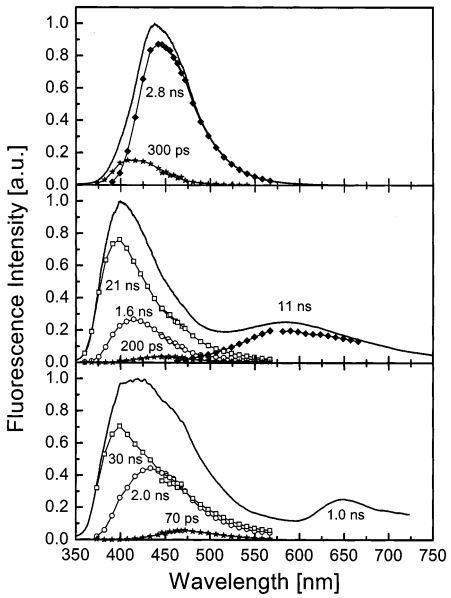

Figure 6. Decay associated spectra (DAS) obtained for **5** in different solvents with $\lambda_{ex} = 277$ nm: (top) cyclohexane, (middle) CH_2Cl_2, and (bottom) acetonitrile. The spectrograph settings were chosen to yield overlapping spectral regions.

where $F(\lambda_j)$ represents the steady-state spectral distribution and A_i and τ_i are the parameters derived by the global fit procedure for the assumed multiexponential fluorescence decay law $R(\lambda_j,t)$:

$$R(\lambda_j,t) = \sum_{i=1}^{3} A_i(\lambda_j) \exp(-t/\tau_i)$$

The DAS calculated for the various fluorescence components in different solvents exhibit interesting features with respect to spectral distribution (Figures 6 and 7). The maximum of the DAS of the longest-lived component ($\tau > 20$ ns) found for **5** is at about the same wavelength in CH_2Cl_2 and acetonitrile, around 400 nm, and matches well the fluorescence maximum of phenyl-substituted pyrene, whose fluorescence spectrum shows only a weak vibrational structure, Figure 1a. It appears, however, that the long-wavelength tail extends further to the red.

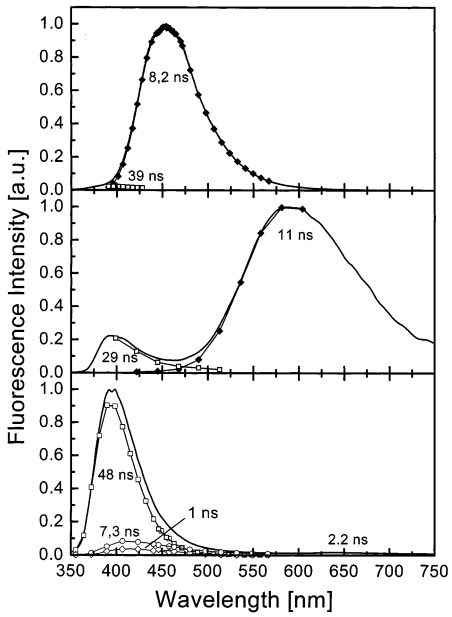

Figure 7. Decay associated spectra (DAS) obtained for **4** in different solvents with $\lambda_{ex} = 277$ nm: (top) cyclohexane, (middle) CH_2Cl_2, and (bottom) acetonitrile. The spectrograph settings were chosen to yield overlapping spectral regions.

The DAS connected with the second decay time of **5** in the blue spectral region shows a small, but significant, bathochromic shift (approximately 15 nm) on switching from CH_2Cl_2 to acetonitrile. Such a shift could be caused by solvent relaxation, if the emitting state possesses a large dipole moment, or by solvent-dependent geometrical relaxation of the solute. Evidence for the existence of the latter processes could eventually be seen in the appearance of a third decay time. The derived values ($\tau < 300$ ps), however, match those found in the pump−probe experiments of **5** (325 ps in methylcyclohexane, 140 ps in methyl THF, and 80 ps in acetronitrile),[17] where they were assigned to structural relaxation in the CT state.

In derivative **4**, the blue emission is dominated by the DAS of the longest-lived component, which matches to a large extent the fluorescence spectrum of phenylpyrene. Additionally, evidence for two small components with decay times of 7.3 ns and about 1 ns could be found in acetonitrile.

The DAS of the various fluorescence components observed in CH_2Cl_2 and acetonitrile are in accord with the assignment of the blue emission as originating from LE states and the red emission from a CT state. The differences between the fluorescence lifetimes of the model compounds **1** and **2** and the lifetimes determined by the analysis of the blue emission contradict the suggestion that the latter is caused by traces of phenyl-substituted pyrene or phenothiazine.

It has been mentioned above that the steady-state fluorescence spectra of **4** and **5** in cyclohexane are significantly different. The analysis of the time-resolved data shows that in the meta derivative **4** the whole spectrum is governed by only one component with a decay time $\tau_1 = 8.2$ ns. An extremely small second component with $\tau_2 = 39$ ns is only found at the blue end. In contrast, in the para derivative **5** a significant second component is found with a very short decay time ($\tau_2 \sim 300$ ps). The lifetime of the dominant component is only 2.8 ns, the maximum of the corresponding DAS around 445 nm. Both data suggest a correlation with fluorescence from phenothiazine. Noteworthy is furthermore that the DAS of the dominant component of **4** and **5** exhibits a nearly perfect match of the blue edge, whereas the red edge is shifted bathochromically in

4. This might indicate that in **4** the emission spectrum represents a superposition of the fluorescence from a locally excited phenothiazine and a nearby CT state. For both states to decay with one common decay time, it is necessary that a rapid equilibrium between them be established.

3.3. Thermodynamic Considerations for the Majority Species. If one accepts the hypothesis that the compounds investigated can exist in solution as different conformers, then the question arises as to the nature of these conformers. We mentioned above that in a previous publication we postulated that the majority species, which undergoes ultrafast photoinduced electron transfer, exhibits the same geometry in solution as found by X-ray analysis of crystalline material. Using these structural data, one can estimate via the Rehm−Weller equation the change in Gibbs energy upon formation of the CT state, ΔG_{et}:[17]

$$\Delta G_{et} = e(E_{ox}(D) - E_{red}(A)) - E_{0,0} - \frac{e^2}{4\pi\epsilon_0\epsilon R_{DA}} + C$$

with $E_{ox}(D)$ and $E_{red}(A)$ being the oxidation potential of the donor and reduction potential of the acceptor group, respectively. R_{DA} represents the distance across which the electron is transferred. C compensates for entropy changes and was estimated to be on the order of 0.1 eV.[17] The results, which are summarized in Table 1, suggest that with the geometry of the assumed majority conformer a complete electron transfer is a strongly exergonic process in CH_2Cl_2 and acetonitrile. In cyclohexane, ΔG_{et} is only slightly negative for the assumed geometry. This implies that small geometric changes could reduce the driving force even further, without taking into account that the approximations involved mean that the estimate could in any case be in error by ± 0.2 eV.

If the energetic separation between the LE and the CT states is of the order of k_BT (as assumed to be the case in nonpolar solvents), then thermally induced back electron transfer to recreate a locally excited state (possibly with a slightly different geometry) could give rise to delayed LE-type fluorescence. With the rate constants for charge separation and recombination being sufficiently high to guarantee an equilibrium population for the two involved states, the fluorescence decay should be monoexponential after equilibrium has been established. The spectral distribution would correspond to a weighted superposition of the inherent LE and CT fluorescence.

3.4. Search for the Minority Conformation. Following the model proposed above, we expect the rate of photoinduced electron transfer, k_{et}, in the minority conformation to be much smaller than the rate constants for radiative and nonradiative relaxation to the electronic ground state. The rate k_{et} depends on the electronic coupling matrix element, H_{RP}, and the Franck−Condon weighted density of states FCWD:[20]

$$k_{et} = \frac{2\pi}{\hbar} H_{RP}^2 \,\mathrm{FCWD}$$

Therefore, the required reduction of the rate k_{et} in the minority versus the majority species can, in principle, be due either to a strong decrease in FCWD, since FCWD depends on ΔG_{et}, or to a much smaller electronic coupling. In terms of the Rehm−Weller equation the former possibility could be rationalized if a change in the hybridization of the (donating) lone pair at the nitrogen changes the ionization potential of the phenothiazine donor. The latter possibility could work for two reasons. First, the coupling between donor or acceptor and the bridge can become smaller, e.g., by rotation of the connecting single bonds.

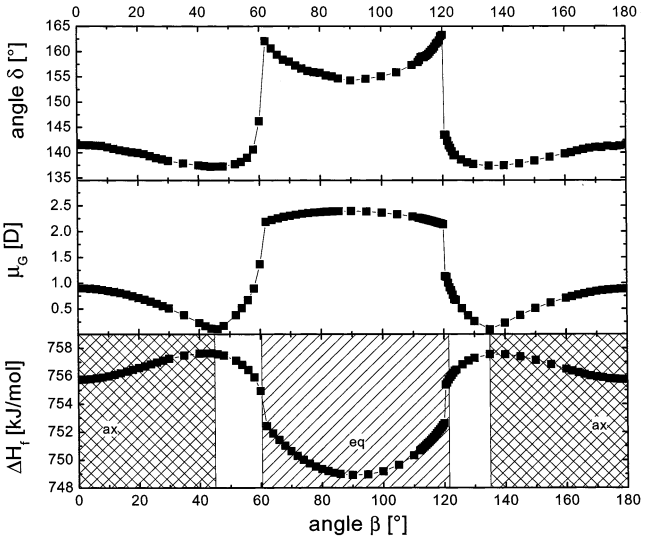

Figure 8. Results obtained for **5** from quantum chemical model calculations employing the AM1 Hamiltonian for the heat of formation (ΔH_f), the dipole moment in the electronic ground state (μ_G), and the dihedral angle δ, which describes the deviation from planarity of the phenothiazine moiety. The angle β describes phenylphenothiazine single bond rotation (all other geometrical parameters are optimized).

Alternatively, the ordering of the molecular orbitals could change in response to geometrical changes. This implies that certain MO's, when acting as HOMO and LUMO, couple strongly, whereas other combinations do not. As a further consequence of an energetic rearrangement of the MO's, one can also imagine that the energetic ordering of the molecular eigenstates is changed such that a state with CT character is higher in one and lower in the other conformer than the lowest LE state.

In pursuing the already mentioned hypothesis of different conformers, we deliberately fixed the angle β (rotation of the single bond connecting phenothiazine to the phenyl bridge, see also Scheme 1) when searching for the minimum energy geometry.The results of this procedure in the case of **5** are shown in Figure 8. The plot of the heat of formation ΔH_f versus β exhibits a wide range of low-energy conformations with $60° < \beta < 120°$. In a second range, $135° < \beta < 225°$, ΔH_f is about 7 kJ mol^{-1} higher. Under the assumption that the entropy of both conformers is essentially equal, we obtain a population ratio of about 12:1 for these two types of conformers. For the para-derivative **5**, the dependencies shown are symmetrical for angles β and $-\beta$. In the case of **4**, similar variations of ΔH_f, μ_G, and δ are found, although with a slight asymmetry of the barrier height around $\beta = 130°$ and 230°. The energy-optimized geometries calculated for derivatives **4** and **5** in the quasi-equatorial and quasi-axial conformation are shown in Figure 9.

Inspection of Figures 8 and 9 also reveals that torsion around the single bond connecting phenothiazine to the phenyl bridge affects the planarity of the phenothiazine moiety. The latter is quantified by the angle δ between the two planes defined by C^1C^2N and C^2NC^3, as indicated in Scheme 1. In the minimum energy conformation (which represents the quasi-equatorial conformation), the deviation from planarity is less than in the second conformer (the quasi-axial conformation). It is obvious that such changes in geometry must affect the excitation energy of those states that are essentially localized on the phenothiazine moiety. Furthermore, the ionization potential (of the nitrogen lone pair) of the phenothiazine moiety will be affected, thus making estimates via the Rehm−Weller equation less reliable.

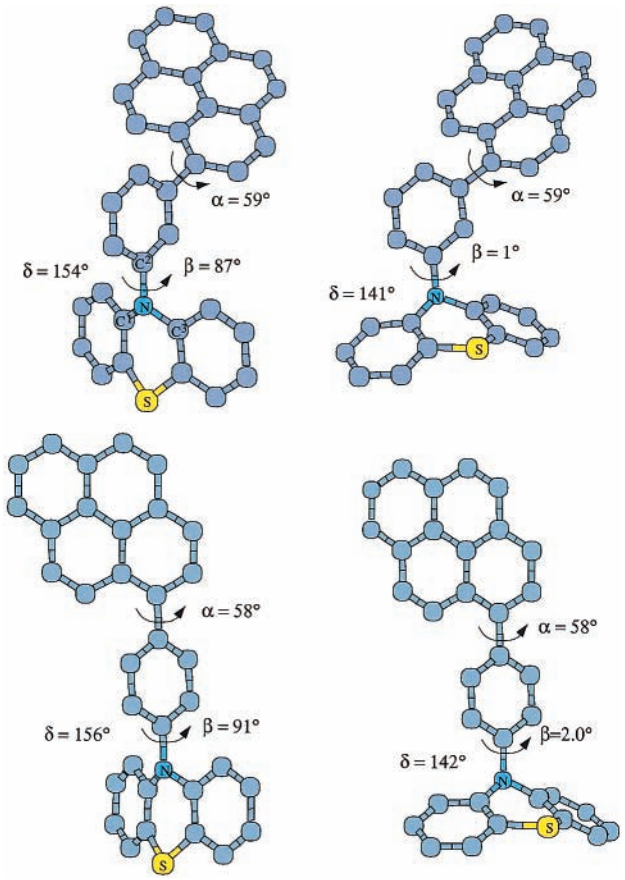

Figure 9. Geometries of the two relevant conformers of **4** and **5** as proposed by quantum chemical model calculations employing the AM1 Hamiltonian: (left) quasi-equatorial and (right) quasi-axial. Angles α and β denote the rotation around the single bonds, and δ denotes the angle between the planes spanned by atoms C^1C^2N and C^2NC^3, respectively.

According to the quantum chemical model calculations, the difference in ionization energy of majority and minority species amounts to about 0.46 eV.

3.5. Quantum Chemical Modeling of Excited States (Franck−Condon States). As expected from the discussion above, the quantum chemical calculations (gas phase) yield different molecular orbital schemes for the two conformers (Figures 10 and 11). In the predominant, quasi-equatorial, conformer of the para-substituted derivative **5**, HOMO and LUMO are strongly localized on phenothiazine (donor) and phenylpyrene (acceptor), respectively. According to the common, but oversimplified, one-electron concept, the HOMO → LUMO transition would represent a nearly complete charge-transfer excitation with a very low extinction coefficient. The CI calculations predict the HOMO → LUMO transition to make a major contribution to the S_5 state only and to cause a large change in dipole moment (Table 3a). One-electron promotion from HOMO-1 or HOMO-3 to LUMO contributes to locally excited states of phenylpyrene. The latter transitions (including those to LUMO+1) establish the second excited state (Table 3a), with a large oscillator strength *f* and the close-by lying S_3 state with low *f*. The first excited singlet state (λ_{ex} = 416 nm) with very low oscillator strength should, according to the calculations, be responsible for the long wavelength absorption tail. It mainly represents the excitation of phenylphenothiazine but has also some CT character. The involvement of the AO's located at the pyrene moiety in L+2 and L+3 explains why in phenylphenothiazine this transition does not appear in the same way. Internal conversion from the preferentially excited S_2 state (largest oscillator strength) to the S_1 state would correspond to an energy transfer from pyrene to phenothiazine but not to a more or less complete electron transfer (pyrene radical anion and phenothiazine cation). The latter is possible only if the calculated CT states (S_5 or S_{10}) are stabilized enough by the solvent that they lie below the essentially locally excited phenothiazine state. This is likely despite the high calculated energies, since the CI calculations used tend to overestimate the energy needed for charge separation (see below).

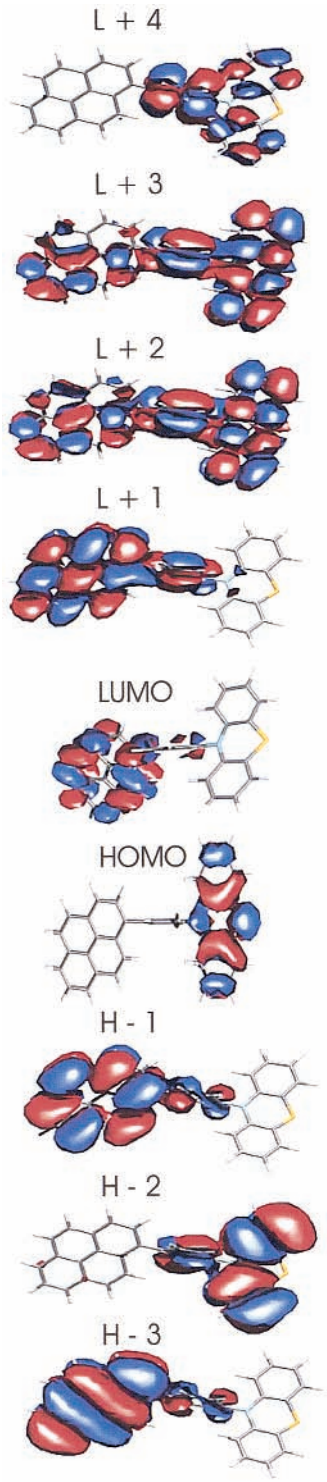

Figure 10. Schematic of the molecular orbitals involved in the CI description of the excited states of the quasi-equatorial conformer of **5** (gas-phase calculations).

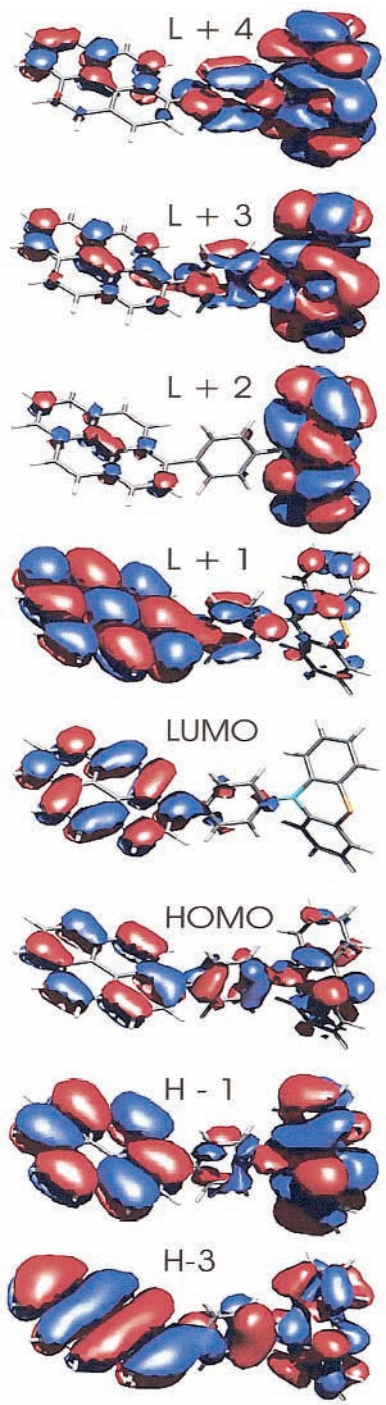

Figure 11. Schematic of the molecular orbitals involved in the CI description of the excited states of the quasi-axial conformer of **5** (gas-phase calculations).

For the quasi-axial conformer, the calculations predict three close lying excited states in the wavelength range $360 < \lambda < 340$ nm. However, only one of these, S_2, has a large oscillator strength (Table 3b). From the MO pictures shown in Figure 11, one would characterize this transition as being mainly localized on the phenylpyrene moiety. Despite a significant contribution of phenothiazine atomic orbitals in HOMO-3 and HOMO-1, there is only a small charge transfer from phenothiazine to pyrene connected with this transition. In analogy to the situation in the quasi-equatorial conformer, internal conversion from the primarily excited S_2 state to the close lying S_1 state again causes only a small charge rearrangement. In contrast to the quasi-equatorial conformer, the calculations predict, however, no CT state within a reasonable energy gap to the ground state. This means that in the quasi-axial conformer no CT state should exist below the lowest locally excited state, not even in the most polar solvents available.

TABLE 3: Excited State Properties Predicted by Quantum Chemical Model Calculations for Compound 5

state	λ_{ex}, nm	f	$\Delta\mu$, D	character	involved config
(a) Quasi-equatorial Conformer of **5** (Majority Species)					
S_1	415	0.002	2.9	LE Phtz	H → L+3, H → L+2
S_2	348	0.348	0.2	LE Py	H-1 → L, H-3 → L+1
S_3	340	0.003	0.3	LE Py	H-3 → L, H-1 → L+1
S_5	290	0.004	23	CT	H → L, H → L+2 H-1 → L+3
S_{10}	235	0.250	37	CT	H → L
(b) Quasi-axial Conformer of **5** (Minority Species)					
S_1	359	0.093	3.9	LE Phtz	H → L+2, H-1 → L+2
S_2	356	0.410	0.2	LE Py	H-3 → L+1, H-1 → L
S_3	348	0.006	0.54	LE Py	H → L+1, H-3 → L

TABLE 4: Excited State Properties Predicted by Quantum Chemical Model Calculations for Compound 4

state	λ_{ex}, nm	f	$\Delta\mu$, D	character	involved config
(a) quasi-equatorial conformer of **4** (majority species)					
S_1	417	0.001	2.9	LE Phtz	H → L+2, H → L+3
S_2	347	0.181	0.1	LE Py	H-1 → L, H-3 → L+1
S_3	340	0.003	0.2	LE Py	H-1 → L+1, H-3 → L
S_6	270	0.035	26	CT	H → L, H → L+4, H-2 → L+3
S_{10}	236	0.322	32	CT	H → L,H → L+4
(b) quasi-axial conformer of **4** (minority species)					
S_1	351	0.105	4.1	LE Phtz	H → L+2
S_2	344	0.140	0.4	LE Py	H-1 → L, H-3 → L+1
S_3	339	0.007	0.7	LE Py	H-1 → L+1, H-3 → L
S_4	326	0.187	3.1	LE phenyl-PTZ	H → L+3, H → L+4

For the meta-substituted derivative **4**, the quantum chemical calculations predict an analogous situation with respect to the nature of the electronically excited states (Table 4) as in the para-derivative **5**. Again, one finds that in the quasi-equatorial conformer the highest occupied orbitals are localized either on the pyrene or phenothiazine moiety, whereas in the quasi-axial conformer, the phenyl AO's contribute to MO's preferentially localized on the phenothiazine.

3.6. Stabilization of CT States by Solvent and Geometrical Relaxation. To elucidate the geometrical relaxation processes postulated on the basis of the existence of very short-lived components in both the fluorescence decay curves and the transient absorption spectra, we employed a newly developed geometry optimization algorithm to search for those molecular geometries which represent minima of the excited-state hypersurfaces (in vacuo).

Optimization of the first singlet exited state starting from the minority species of **5** leads to two minima. The geometry of the first one (structure **A** in Figure 12) differs from the starting geometry only by a more planar nitrogen ($\delta = 175°$). The second, fully relaxed structure (B, Figure 12) exhibits an essentially planar phenothiazine moiety. Whereas the angle α

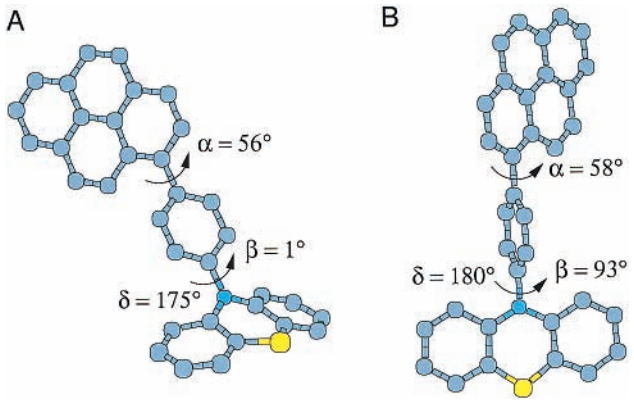

Figure 12. Structures of the partially (A) and fully (B) relaxed lowest excited singlet state of **5**. (For more details see text.)

stays around 57°, angle β is increased to 90°. If one takes the geometry of the majority (quasi-equatorial) species as starting point, optimization leads directly to structure **B**.

Further examination of the excited states of **5** reveals *two* CT-states, the lower of which has about half the dipole moment of the higher. Optimization of these states leads to two different structures, which we have labeled "bridge charge transfer" (BCT) and "acceptor charge transfer" (ACT), respectively. The BCT state adopts a geometry in which the phenyl bridge is perpendicular to the phenothiazine ring system but in which the pyrene is only twisted by 48° relative to the phenyl bridge. The sum of the Coulson charges on the phenothiazine system is $+0.84$ e$^-$ but only -0.18 e$^-$ on the pyrene rings, leaving -0.66 e$^-$ for the bridging phenyl group. The calculated gas-phase dipole moment is 21.1 D. Figure 13 shows the structure and the calculated molecular electrostatic potential at the surface of the molecule for this state. The phenothiazine ring system is clearly oxidized, but the negative charge is centered on the phenyl−pyrene bond, rather than on the formal pyrene acceptor. BCT thus shows almost complete (84%) charge transfer, but over a shorter range than expected for the full donor (phenothiazine)−acceptor (pyrene) charge-transfer state.

The second charge-transfer state, ACT, adopts a geometry in which the phenyl bridge is perpendicular to both the phenothiazine and the pyrene ring systems. The calculated total Coulson charge on the phenothiazine is $+0.86$ e$^-$, but the total Coulson charge on the pyrene unit is now -0.99 e$^-$, indicating complete transfer of one electron to the acceptor group with some delocalization of the positive charge (13%) into the bridging phenyl group from the phenothiazine donor. The calculated dipole moment of this state is 45.2 D. Figure 13 shows the structure and molecular electrostatic potential of this state. The complete charge transfer from the donor to the acceptor separated by the phenyl bridge, which is perpendicular to both redox active groups, can be seen clearly. The meta-linked compound **4** shows exactly analogous BCT and ACT states.

Single-point calculations on the relaxed S_1 states, the Franck−Condon S_1 states, and the relaxed structures for the BCT and ACT charge transfer states in the simulated solvents hexane ($\epsilon = 2.023$), *n*-hexadecane (2.050), CCl_4 (2.229), benzene (2.274), ether (4.197), chloroform (4.806), methylene chloride (8.93), acetone (20.56), ethanol (24.55), methanol (32.66), acetonitrile (35.94), dimethyl sulfoxide (46.45), and water (78.36) were then performed in order to judge the solvent effects on the relative stabilities of the different states for compounds **4** and **5**. The results are shown in Figure 14. Our experience[40] suggests that CT states are calculated to be too unstable relative to LE states with the techniques used but that the relative

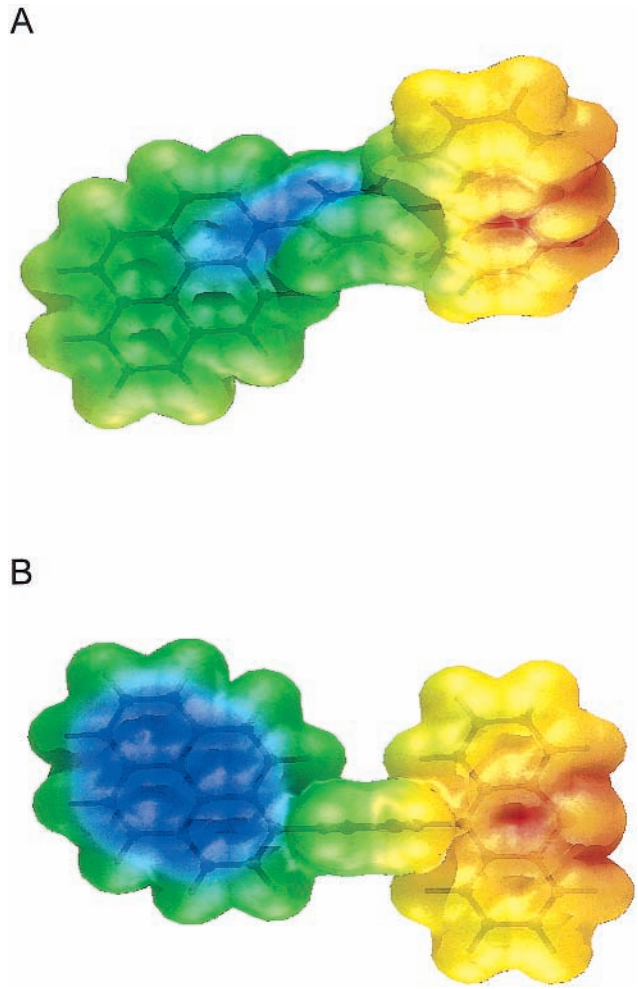

Figure 13. Geometry and molecular electrostatic potential of the "bridge CT" (A) and "acceptor CT" state (B) of **5**.

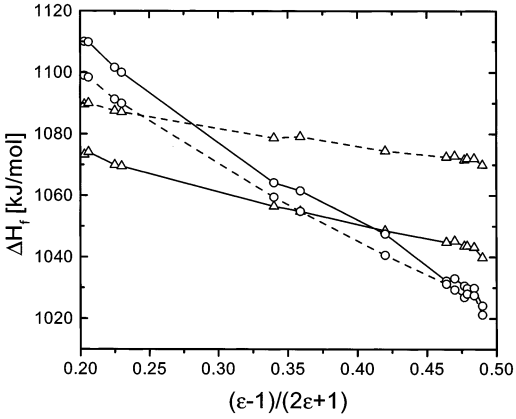

Figure 14. Dependence of the calculated heats of formation, ΔH_f, for the various discussed CT states on solvent permittivity: BCT of **4** (- -○- -) and **5** (−○−) and ACT of **4** (- -△- -) and **5** (−△−).

energies of different CT states and conformations and their solvent dependence are reproduced remarkably well.

Figure 14 suggests that the major difference between compounds **4** and **5** is that the BCT state in the para-bridged compound **5** is more stable relative to both the S_1 and the ACT states. The energies of the S_1 states, which are nearly independent of solvent polarity, are remarkably similar for the two isomers and the ACT state is marginally more stable for the meta-bridged **4** than for **5**, as might be expected from the slightly shorter charge separation distance. The crossing between the

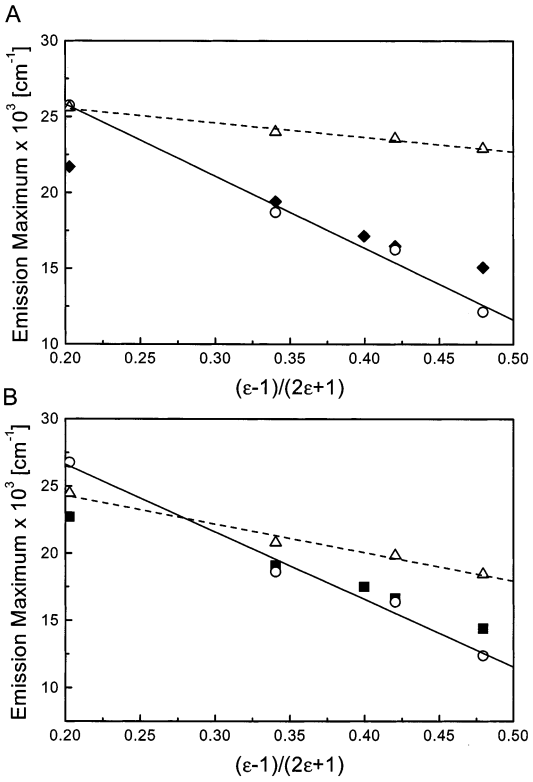

Figure 15. Comparison of the dependence of the experimental and the calculated transition energies from the CT state to the Franck−Condon ground state on solvent polarity parameter for **4** (A) and **5** (B). (experimental values: ♦, ■; BCT: △, --; ACT: ○, -).

two CT states occurs for nonpolar solvents for **4** but at about the polarity of methylene chloride for **5**. This crossing suggests that the identity of the CT state responsible for the fluorescence in **5** should change from BCT at lower solvent polarities to ACT for polar solvents. To test this hypothesis, we have plotted the observed fluorescence maxima for **5** (and **4**) against those calculated for the BCT and CT states but have corrected the calculated values downward by 3000 cm^{-1} (0.37 eV) to account for the underestimation of ACT state stabilities in the calculations. The results are shown in Figure 15 B. Although not conclusive, especially for the polar solvents, the figure suggests that the nonlinearity observed in the Lippert−Mataga plot for **5** (Figure 4) may indeed result from the change in the nature of the fluorescing CT state. A corresponding plot for the meta-bridged compound **4** is shown in Figure 15A. In this case the data can be fitted relatively well using only the ACT state and the same correction factor as for **5**. The point for the cyclohexane solvent deviates significantly, however, so that the BCT state may actually also be important for this compound. The calculations, however, provide a convincing explanation for the observed behavior of **4** and **5**.

3.7. The Origin of the Red and Blue Emission Band. In moderately polar (CH_2Cl_2) and polar solvents (acetonitrile), the red emission band can unequivocally be attributed to an excited state with fairly high dipole moment. Since its decay time matches that of the transient absorption assigned to the radical ion pair,[17] the red fluorescing species must be the majority species. According to the quantum chemical calculations, it is the quasi-equatorial conformer which is, for both **4** and **5**, the thermodynamically most stable ground state species. Internal conversion from the primarily excited higher electronic state with pyrene LE character to the solvent-stabilized lowest excited state with charge-transfer character (phenothiazine to pyrene) is followed by fast barrierless geometrical relaxation leading to a twisted internal charge-transfer state. The initial charge separation process occurs on the time scale of 10 ps, as shown by pump−probe and time-resolved Raman experiments. Therefore, the rise of the CT emission is beyond the time resolution of the fluorescence experiment.

The photophysical behavior of the minority species, the quasi-axial conformer, is somewhat different in the meta- and para-substituted derivatives. Time-resolved fluorescence spectra recorded for phenylphenothiazine show a change in spectral distribution (bathochromic shift of maximum by 40 nm) during the first hundred picoseconds after excitation.[26] We therefore hypothesize that the subnanosecond component observed for **5** (in all solvents) is related to geometrical relaxation and could cause a more effective decoupling of the π-electronic system of the phenylpyrene moiety from that of phenothiazine. The excitation on either of the two subunits appears to decay essentially independently: the barely quenched excited phenylpyrene moiety, in analogy to **1**, gives rise to the fluorescence with a maximum around 400 nm, the phenothiazine subunit emits, depending on solvent polarity, with its maximum between 415 and 440 nm. The solvatochromism of the phenothiazine fluorescence causes the unusual broadness of the blue emission band in acetronitrile.

The postulate of barely quenched phenylpyrene fluorescence contradicts the intuitive assumption of an ultrafast energy transfer between two chromophores located within a short center-to-center distance. In the formula usually used for nonradiative energy transfer[41]

$$k_{DA} = \frac{9(\ln 10)\kappa^2 \Phi_D I_{DA}}{128\pi^5 N_A n^4 \tau_D^0 R_{DA}^6}$$

the system specific parameters are

(i) I_{DA} = the spectral overlap between donor fluorescence and acceptor absorbance,

(ii) τ_D^0 = the donor fluorescence lifetime in the absence of quencher, and

(iii) $\kappa = (\cos \Theta_{DA} - 3 \cos \Theta_D \cos \Theta_A)$ the orientation factor (Θ_{DA} represents the angle between the transition moment of donor and acceptor; Θ_D and Θ_A represent the angle between the transition dipole moments and the distance vector).

Inspection of Figure 1 shows that the overlap integral I_{DA} is very small for the pair phenylpyrene and phenylphenothiazine; furthermore, the lifetime of phenylpyrene is rather large (∼100 ns). Consequently, energy transfer should not be too efficient even if κ^2 is at its maximum value (for $\Theta_{DA} = 0$, $\Theta_D = \Theta_A = 90°$). In our phenyl-bridged systems, the relative orientation of the transition dipole moments changes with geometrical relaxation. It is therefore difficult to make an appropriate estimate, even if one ignores that the above formula for κ is valid only for donor−acceptor distances that are large compared to the molecular dimensions. Consequently we have evaluated the more appropriate expression[42]

$$\hat{\kappa} = \frac{1}{m_D m_A} \sum_{j \in A} \sum_{i \in D} \frac{q_i^* q_j^*}{r_{ij}}$$

with m_D, m_A being the transition dipole moments and q_i^*, q_j^* the transition charges of the donor and acceptor, respectively.

The results are in accordance with expectation in that κ^2 varied between 0.01 and 1 for different assumed conformations. In summary, it seems very reasonable that, depending on the actual situation, the lifetime of the excited phenylpyrene moiety is reduced to 20−50 ns by energy transfer to phenothiazine.

Because the lifetime of excited phenothiazine is comparatively short, the fluorescence contribution induced by excitation via energy transfer can be small and therefore does not lead to a detectable component with negative amplitude. Energy transfer possibly manifests itself in the fact that the DAS of the 20−40-ns component extends further to the red than the fluorescence spectrum of phenylpyrene. In view of the complexity of the molecule/solvent system investigated, we do not feel justified in assigning the short-lived fluorescence component definitively. Further high-pressure and/or low-temperature experiments will be needed to clarify this point.

The fluorescence behavior in nonpolar solvents is governed by the energetics of the CT states, as mentioned above in connection with the estimates via the Rehm−Weller equation. In the para-derivative **5**, the acceptor CT state, ACT, should be higher in energy than the bridge CT state, BCT (Figure 14). This implies that charge transfer should stop at the level of the BCT state. In the meta-derivative, the two CT states are of similar energy. Whether the ACT state is reached or not also depends on the barrier in between. We can rationalize the observed fluorescence behavior if we assume that in case of **4** the BCT state is reached but does not efficiently react further to the ACT state. Instead, back electron transfer may become operative to create a LE state with a geometrically slightly modified phenothiazine. If the equilibrium population of these two states is established fast, then both states decay uniformly, the spectral distribution of the fluorescence being a weighted average of the emission spectra of both states.

In the case of the para-derivative **5**, the BCT state is somewhat higher in energy than the corresponding LE state of phenothiazine. Although it is formed with lower efficiency from the higher electronically excited LE states, it cannot decay efficiently to the still higher lying ACT state. Instead, back electron transfer occurs to the phenothiazine LE state, from which the observed fluorescence is emitted. In the proposed model, the recorded fluorescence should be nearly exclusively due to the majority species. Contributions from the minority conformer should be difficult to detect since its spectral properties are very close to those of the majority species.

4. Summary and Conclusion

We have provided strong evidence that the donor−bridge−acceptor systems investigated can exist in solution as different conformers with dramatically different photophysical properties. In the majority of species, internal conversion from the primarily excited higher electronic states with LE character to the solvent-stabilized lowest excited singlet state is connected with a significant charge transfer from phenothiazine to pyrene. In moderately and very polar solvents, barrierless geometrical relaxation occurs (rotation around connecting single bonds and planarization of phenothiazine moiety), thereby ending up in a kind of twisted internal charge transfer (TICT) state. Consequently, the emission from this relaxed state exhibits a large solvatochromic effect, as is typical for emission from such charge-transfer states. For the minority species, the photophysical properties depend somewhat on the substitution pattern of the bridging phenyl ring. Similar relaxation processes occur, but the final, relaxed state has no pronounced charge-transfer character. The fluorescence therefore resembles that of either one (or both) of the constituting building blocks.

The interpretation of the fluorescence behavior in nonpolar solvents is most difficult. Transient absorption and Raman data provide evidence that charge transfer occurs in the meta-derivative **4**. This implies that most of the fluorescence signal should orginate from the majority species. Since the spectral distribution is close to that of phenothiazine, we assume, in accordance with the theoretical predictions, that an equilibrium is established between the CT state and the LE state of phenothiazine. If the rates for conversion are fast, then the two states decay uniformly. This assumption could also explain why this state decays faster than the pure CT state formed in moderately polar solvents despite the larger energy gap.

In the para-derivative, for energetic reasons the CT state is formed with lower efficiency, because it is less stable than the LE state from which fluorescence occurs with a lifetime typical for phenothiazine. The appearance of the 300-ps component should be related to the relaxation of the originally formed CT state, which is also radiatively coupled to the ground state. Consequently, the transient absorption spectrum contains significant contributions from the excited-state absorption of phenothiazine.

Our calculations clearly show the existence of a bridge charge transfer state in which the phenyl bridge plays an active role as acceptor. In a more extended system, this type of state is analogous to a bridge-centered polaron. The existence of such states, however, is intimately connected with torsional relaxation in D−B−A systems.

The fluorescence data presented show that consideration of geometrical relaxation is important for explaining the photophysical parameters of nonrigid systems. In previous studies,[18] we were able to show that applying high pressure helps to quantify the relaxation processes, since solvent permittivity and viscosity can thereby be changed without changing intermolecular interaction. Therefore, further work is presently in progress to gain more insight in the complex behavior, especially in nonpolar solvents.

Acknowledgment. Valuable discussion and technical advice by Dr. K. Kemnitz (EuroPhoton, Berlin) is gratefully acknowledged, as is financial support by Volkswagen-Stiftung, Deutsche Forschungsgemeinschaft, and Fonds der Chemischen Industrie. We also thank one of the reviewers for his critical and very valueable comments.

References and Notes

(1) (a) Paddon-Row, M. N. *Acc. Chem. Res.* **1994**, *27*, 18. (b) Wasielewski, M. R. *Chem. Rev.* **1992**, *92*, 435. (c) Gust, D.; Moore, T. A.; Moore, A. L. *Acc. Chem. Res.* **1993**, *26*, 198.

(2) (a) Lawson, J. M.; Paddon-Row: M. N.; Schuddeboom, W.; Warman, J. M.; Clayton, A. H. A.; Ghiggino, K. P. *J. Phys. Chem.* **1993**, *97*, 13099. (b) Roest, M. R.; Verhoeven, J. W.; Schuddeboom, W.; Warman, J. M.; Lawson, J. M.; Paddon-Row, M. N. *J. Am. Chem. Soc.* **1996**, *118*, 1762. (c) Lauteslager, X. Y.; van Stokkum, I. H. M.; van Ramesdonk, H. J.; Bebelaar, D.; Fraanje, J.; Goubitz, K.; Schenk, H.; Brouwer, A. M.; Verhoeven, J. W. *Eur. J. Org. Chem.* **2001**, 3105. (d) Hviid, L.; Brouwer, A. M.; Paddon-Row: M. N.; Verhoeven, J. W. *Chem. Phys. Chem.* **2001**, *4*, 232.

(3) (a) Greenfield, S. R.; Svec, W. A.; Gosztola, D.; Wasielewski, M. R. *J. Am. Chem. Soc.* **1996**, *118*, 6767. (b) Debreczeny, M. P.; Svec, W. A.; Marsh, E. M.; Wasielewski, M. R. *J. Am. Chem. Soc.* **1996**, *118*, 8174. (c) Debreczeny, M. P.; Svec, W. A.; Wasielewski, M. R. *Science* **1996**, *274*, 584. (d) Gosztola, D.; Niemczyk, M. P.; Wasielewski, M. R. *J. Am. Chem. Soc.* **1998**, *120*, 5118. (e) Lukas, A. S.; Miller, S. E.; Wasielewski, M. R. *J. Phys. Chem. B* **2000**, *104*, 931.

(4) (a) Zimmermann, S. C.; Zeng, Z.; Wu, W.; Reichert, D. E. *J. Am. Chem. Soc.* **1991**, *113*, 183. (b) Zimmermann, S. C.; Wu, W.; Zeng, Z. *J. Am. Chem. Soc.* **1991**, *113*, 196.

(5) (a) Klärner, F.-G.; Burkert, U.; Kamieth, M.; Boese, R.; Benet-Buchholz, J. *Chem. Eur. J.* **1999**, *5*, 1700. (b) Klärner, F.-G.; Panitzky, J.; Preda, D.; Scott, L. T. *J. Mol. Model.* **2000**, *6*, 318. (c) Kamieth, M.; Burkert, U.; Corbin, P. S.; Dell, S. J.; Zimmermann, S. C.; Klärner, F.-G. *Eur. J. Org. Chem.* **1999**, *2741*, 1.

(6) Nelson, S. F. *Chem. Eur. J.* **2000**, *6*, 581.

(7) (a) Kurebayashi, H.; Fukazawa, Y. *Chem. Lett.* **2000**, 530. (b) Kurebayashi, H.; Sakaguchi, M.; Okajima, T.; Haino, T.; Usui, S.; Fukazawa, Y. *Tetrahedron Lett.* **1999**, *40*, 5545.

(8) Kurreck, H.; Huber, M. *Angew. Chem., Int. Ed. Engl.* **1995**, *34*, 849.

(9) (a) Kumar, K.; Lin, Z.; Waldeck, D. H.; Zimmt, M. B. *J. Am. Chem. Soc.* **1996**, *118*, 243. (b) Read, I.; Napper, A. M.; Kaplan, R.; Zimmt, M. B.; Waldeck, D. H. *J. Am. Chem. Soc.* **1999**, *121*, 10976.

(10) (a) Carter, F. L.; Siatkowski, R. E.; Wohltjen, H., Eds. *Molecular Electronic Devices*, Elsevier: Amsterdam, 1988. (b) Mahler, G., May, V., Schreiber, M., Eds. *Molecular Electronics−Properties, Dynamics, and Applications;* Marcel Dekker: New York, 1996. (c) Jortner, J.; Ratner, M. A., Eds. *Molecular Electronics*; Blackwell: Oxford, 1997.

(11) Ramsteiner, I. B.; Hartschuh, A.; Port, H. *Chem. Phys. Lett.* **2001**, *343*, 83.

(12) Herbich, J.; Kapturkiewicz, A.; Nowacki, J.; Golinski, J.; Dabrowski, Z. *Phys. Chem. Chem. Phys.* **2001**, *3*, 2438.

(13) Luo, C.; Guldi, D. M.; Imahori, H.; Tamaki, K.; Sakata, S. *J. Am. Chem. Soc.* **2000**, *122*, 6535.

(14) Gong, X.; Ng, P. K.; Chang, W. K. *Adv. Mater.* **1998,** *10*, 1337−1340.

(15) (a) Daub, J.; Beck, M.; Knorr, A.; Spreitzer, H. *Pure Appl. Chem.* **1996**, *68*, 1399. (b) Knorr, A.; Daub, J. *Angew. Chem., Int. Ed. Engl.* **1995**, *34*, 2664. (c) Knorr, A.; Daub, J. *Angew. Chem., Int. Ed. Engl.* **1997,** *36*, 2817. (d) Spreitzer, H.; Scholz, J.; Gescheidt, G.; Daub J. *Liebigs Ann.* **1996**, 2069.

(16) (a) Seischab, M.; Lodenkemper, Th.; Stockmann, A.; Schneider, S.; Koeberg, M.; Roest, M. R.; Verhoeven, J. W.; Lawson, J. M.; Paddon-Row: M. N. *Phys. Chem. Chem. Phys.* **2000**, *2*, 1889. (b) Reek, J. N. H.; Rowan, A. E.; Crossley, M. J.; Nolte, R. J. M. *J. Org. Chem.* **1999**, *64*, 6653. (c) Prathapan, S.; Yang, S. I.; Seth, J.; Miller, M. A.; Bocian, D. F.; Holten, D.; Lindsey, J. S. *J. Phys. Chem. B* **2001**, *105*, 8237. (d) Yang, S. I.; Prathapan, S.; Miller, M. A.; Seth, J.; Bocian, D. F.; Lindsey, J. S.; Holten, D. *J. Phys. Chem. B* **2001**, *105*, 8249.

(17) Daub, J.; Engl, R.; Kurzawa, J.; Miller, S. E.; Schneider, S.; Stockmann A.; Wasielewski, M. R. *J. Phys. Chem. A* **2001**, *105*, 5655.

(18) Bleisteiner, B.; Marian, Th.; Schneider, S.; Brouwer, A. M.; Verhoeven, J. W. *Phys. Chem. Chem. Phys.* **2001**, *3*, 2070.

(19) (a) Verhoeven, J. W.; Wegewijs, B.; Scherer, T.; Rettschnik, R. P. H.; Warman, J. M.; Jäger, W.; Schneider, S. *J. Phys. Org. Chem.* **1996**, *9*, 387. (b) Wegewijs, B.; Ng, A. K. F.; Verhoeven, J. W. *Recl. Trav. Chim. Pays-Bas* **1995**, *114*, 6. (c) Jäger, W.; Schneider, S.; Lauteslager, X. Y.; Verhoeven, J. W. *J. Phys. Chem.* **1996**, *100*, 8118. (d) Lauteslager, X. Y.; van Stokkum, I. H. M.; van Ramesdonk, H. J.; Brouwer, A. M.; Verhoeven, J. W. *J. Phys. Chem.* **1999**, *103*, 653. (e) Jäger, W.; Schneider, S.; Verhoeven, J. W. *Chem. Phys. Lett.* **1997**, *270*, 50.

(20) (a) Marcus, R. *J. Phys. Chem.* **1965**, *43*, 679. (b) Hush, N. S. *Chem. Phys. Lett.* **1988**, *143*, 488. (c) Brunschwig, B. S.; Ehrenson, S.; Sutin, N. *J. Chem. Phys.* **1987**, *91*, 4714.

(21) (a) Bodea, C.; Silberg, I. *Adv. Heterocycl. Chem.* **1968**, *9*, 321. (b) Gupta, R. R. *Phenothiazines and 1,4-Benzothiazines in Bioactive Molecules*; Elsevier: Amsterdam, 1988; Vol. 4.

(22) Borowicz, P.; Herbich, J.; Kapturkiewicz, A.; Opallo, M.; Nowacki, J. *J. Chem. Phys.* **1999**, *249*, 49.

(23) Schneider, S.; Kurzawa, J.; Stockmann, A.; Engl, R.; Daub, J.; Matousek, P.; Towrie, M. *Chem. Phys. Lett.* **2001**, *348*, 277.

(24) Engl. R. Ph.D. Thesis. Universität Regensburg, Germany, 1999.

(25) (a) Kemnitz, K.; Pfeifer, L.; Paul, R.; Fink, F.; Bergman, A. *SPIE Proc.* **1995**, *2628*, 2. (b) Kemnitz, K.; Pfeifer, L.; Paul, R.; Coppey-Moisan, M. *J. Fluorescence* **1997**, *7*, 93. (c) Kemnitz, K.; Paul, R.; Coppey, J.; Coppey-Moisan, M. *SPIE Proc.* **1996**, *2926*, 177. (d) Kemnitz, K.; Pfeifer, L.; Ainbund, M. *Nucl. Instrum. Methods Phys. Res. A* **1997**, *387*, 86.

(26) (a) Stockmann, A. Ph.D. Thesis, Universität Erlangen-Nürnberg, Germany, 2001. (b) Marian, Th. Ph.D. Thesis, Universität Erlangen-Nürnberg, Germany, 2002.

(27) (a) Bevington, P. R.; Robinson, D. K. *Data Reduction and error analysis for the physical sciences*; The Mc-Graw Hill Companies, Inc., Boston; 1992. (b) http://world.std.com/nr. *Numerical Recipies in C*; Cambridge University Press: Cambridge; 1992.

(28) Schneider, S.; Stockmann, A. *Opt. Express* **2000**, *6*, 220.

(29) Fluorescence decay fit program (Fld Fit) for IBM-compatible computers, developed in the course of: Gedeck, P. Ph.D. Thesis, Universität Erlangen-Nürnberg, Germany, 1996.

(30) Clark, T.; Alex, A.; Beck, B.; Burkhardt, F.; Chandrasekhar, J.; Gedeck, P.; Horn, A.; Hutter, M.; Martin, B.; Rauhut, G.; Sauer, W.; Schindler, T.; Steinke, T. Vamp 8.0, Erlangen, 2002.

(31) Dewar, M. J. S.; Zoebisch, E.; Healy, E. F.; Stewart, J. J. P. *J. Am. Chem. Soc.* **1985**, *107*, 3902. Holder, A. J. In *Encyclopedia of Computational Chemistry*; Schleyer, P. v. R., Allinger, N. L., Clark, T., Gasteiger, J., Kollman, P. A., Schaefer, H. F., III, Schreiner, P. R., Eds.; Wiley: Chichester, 1998; Vol. 1, p 8.

(32) Clark, T.; Chandrasekhar, J. *Isr. J. Chem.* **1993**, *33*, 435.

(33) Dewar, M. J. S.; Liotard, D. A. *J. Mol. Struct. (THEOCHEM)* **1990**, *206*, 123.

(34) G. Rauhut, G.; Clark, T.; Steinke, T. *J. Am. Chem. Soc.* **1993**, *115*, 9174.

(35) Gedeck, P.; Schneider, S. *J. Photochem. Photobiol. A: Chem.* **1997**, *105*, 165.

(36) Rauhut, G.; Clark, T. *J. Comput. Chem.* **1993**, *14*, 503. Beck, B.; Rauhut, G.; Clark, T. *J. Comput. Chem.* **1994**, *15*, 1064.

(37) Pascual-Ahuir, J. L.; Silla, E.; Tuñon, I. *J. Comput. Chem.* **1994**, *15*, 1127. Marsili, M.; Floersheim, P.; Dreiding, A. S. *Comput. Chem.*, **1993**, *7*, 175. W. Lorensen, W.; Cline, H. *Comput. Graph.* **1987**, *21*, 163.

(38) Bondi, A. *J. Phys. Chem.* **1964**, *68*, 441.

(39) (a) Lippert, E. *Z. Elektrochem.* **1957**, *61*, 962. (b) Mataga, N.; Kaifu, Y.; Koizumi, M. *Bull. Chem. Soc. Jpn.* **1956**, *29*, 465.

(40) Bleisteiner, B.; Schneider, S.; Clark, T. *J. Mol. Model.* **2002**, *8*, in press.

(41) (a) Förster, Th. *Ann. Physik* **1948**, *2*, 55. (b) Förster, Th. *Fluoreszenz organischer Verbindungen*, Vandenhoeck & Rupprecht, Göttingen 1951.

(42) Le Bret, M.; Le Pecq, J. B.; Barbet J.; Roques, B. P. *Nucleic Acids Res.* **1977**, *4*, 1361.